Desalination and Water Treatment
www.deswater.com

doi:10.5004/dwt.2018.22534

116 (2018) 305–316
June

Experimental and mathematical modelling of reactive dyes decolorization using Fenton oxidation process in a microfluidic system

Hayat Abdulla Yusuf[a,*], Zainab Mohammad Redha[b], Abdulla J. Al Meshal[c], Husain J. Shehab[d]

[a]*Department of Chemical Engineering, College of Engineering, University of Bahrain, P.O. Box 32038, Manama, Kingdom of Bahrain, email: hayousif@uob.edu.bh (H.A. Yusuf)*

[b]*Department of Chemical Engineering, College of Engineering, University of Bahrain, P.O. Box 32038, Manama, Kingdom of Bahrain, email: zali@uob.edu.bh (Z.M. Redha)*

[c]*Technical Services Department, The Bahrain Petroleum Company B.S.C., P.O. Box 25555, Awali, Kingdom of Bahrain, email: ds.almeshaal@hotmail.com (A.J.A. Meshal)*

[d]*Health, Safety and Environment & Continuous Improvement Department, SULB Company B.S.C., P.O. Box 50177, Hidd, Kingdom of Bahrain, email: hshehabi@gmail.com (H.J. Shehab)*

Received 21 February 2018; Accepted 22 May 2018

ABSTRACT

Comprehensive experimental and mathematical studies for reactive dyes decolorization using Fenton oxidation in a microfluidic system were investigated. Reactive Yellow 181 (P2RN/181)and Reactive Blue 19 (RB19), were used as model solutions. The effect of process variables were experimentally and mathematically studied using Design of Experiments(DoE) approach. Mathematical modelling and fluid dynamic studies, using Computational Fluid Dynamics (CFD) modelling on COMSOL software were also implemented to validate the experimental work. Successful decolorization was achieved for both studied dyes in an in-house fabricated T-shaped microfluidic chip with serpentine channels. The DoE approach showed its suitability and effectiveness to optimize the Fenton oxidation process with better performance over previously published work. The optimum operational conditions were found to be 0.8 mM, and 35 mM, for Fe(II) concentration, H_2O_2 concentration, respectively. The highest decolorization percentages in the microfluidic system were found to be 92.9 and 96.0% for RY and RB, respectively at 100 ppm inlet dye concentration, 1.6 mM inlet Fe(II) concentration, and 70 mM H_2O_2 inlet concentration, flowing at a rate of 20 µL/s. CFD results obtained from the microfluidic system revealed 92.8% and 92.3% decolorization efficiencies from RY and RB, respectively after 200 s. The model prediction only deviated by 1.08% (for RY) and 3.85% (for RB) from the experimental values, indicating a very good agreement between the CFD and the experimental results, thereby, successfully validating the proposed model.

Keywords: Fenton oxidation; Reactive dye; Decolorization ; Mathematical modelling; Computational fluid dynamics; Design of experiment; Miniaturization; Microreactor; Microfluidic system

1. Introduction

Decolorization of dyes has been extensively studied in the last few decades, especially for the treatment of waste water from textile industries. Several techniques were developed in this field reflecting the researchers' concern to maintain a clean environment as one of the most important drivers [1–3]. Among those techniques, advanced oxidation using Fenton reagent proved its suitability to produce a good level of dye degradation [4,5]. Fenton reagent in the oxidation process is mainly featured by the activation of hydrogen peroxide without the need for adding energy,

*Corresponding author.

which makes this method cost effective. Oxidation by Fenton is also characterized by its fast rate of decolorization as well as the absence of mass transfer limitation [6]. The main drawback of this technique could be the consumption of substantial amount of oxidant which undoubtedly could be minimized utilizing what is so called miniaturization. With such a technique, other reported drawbacks like long process times and mixing efficiency could also be suppressed.

Chemical processes applied in miniaturized devices have proven significant results in many fields. This is due to the fact that chemical processes performed in microsystems are considered to be economical, efficient, and safe [7]. Moreover, microfluidic systems have high surface area to volume ratios which is 4–5 orders of magnitude greater than the one exist in a regular macro reactor [7]. This eliminates mass transfer limitations and produces a remarkable improvement in the overall reaction rate of processes [8], which could significantly contribute to improving decolorization processes even with less oxidant consumption.

Considering industrial application, miniaturization could also be advantageous as it reduces many issues associated with scaling up of pilot plant studies, especially those related to optimizing industrial plants [9], studying chemical kinetics of processes, as well as both mass and transport phenomena [9,10]. With miniaturization a numbering-up technique could be applied for larger scale industrial applications. This involves having parallel chips operating concurrently to accommodate the large industrial effluents. Such parallel processing is more efficient than installing macro scale systems that require regular maintenance, auxiliary components cost, more operators, and thus, higher labor charges [1,7]. Therefore, it would be worth investigating the capability of dye decolonization in microfluidic systems.

In this study, a T-shaped microfluidic chip (i.e. with two inlets microchannels where two mixing streams are flowed perpendicularly to each other) was fabricated with a serpentine merging channel to investigate its capability to achieve higher decolorization efficiency than in previously published works [11]. In addition, the DoE approach was implemented to introduce efficient optimization of Fenton oxidation process in the fabricated microreactor. Up to the authors' knowledge, this study is considered as the first study for implementing DoE approach, as well as CFD simulation in microfluidic systems for Fenton oxidation [12–14]. The study has shown remarkable results in terms of improvement in the percentage decolorization [11] and the decolorization time [14].

2. Theory

The flow of incompressible Newtonian fluid in miniaturized systems follows Navier-Stokes and could be described by the continuity equations as follows [15]:

$$\partial_t \mathbf{v} + \mathbf{v}\cdot\nabla\mathbf{v} = -\frac{1}{\rho}\nabla P + \nu\nabla^2\mathbf{v} + \mathbf{g} \tag{1}$$

where v is the velocity vector, ρ fluid density, P the pressure, ν the kinematic viscosity and g is the gravitational acceleration, and ∇v = 0. Diffusion and convection describes the transportation of the fluid according to the following dynamic equation [15]:

$$\partial_t c_i + \mathbf{v}\cdot\nabla c_i - D_i\nabla^2 c_i = R_i \tag{2}$$

where c_i, D_i, and R_i are the concentration, diffusion coefficient, and rate of consumption/generation of species i, respectively. For steady-state study, the accumulation terms diminish to zero (i.e. $\partial_t v = \partial_t c_i = 0$).The diffusion coefficient (cm²/s) can be estimated using the empirical Wilke-Chang equation [16]:

$$D_i = \frac{7.4\times10^{-8}\left(\phi_B M w_B\right)^{1/2} T}{\mu_B \upsilon_A^{0.6}} \tag{3}$$

where ϕ_B is the solvent association factor (ϕ_B = 2.6 for water), Mw_B is the molecular weight of solvent (water in this case), T is the temperature (K), μ_B is the solvent viscosity (cP), and ν_A is the dye molar volume (cm³/mol) at its normal boiling point.

Reynolds number plays a major role in defining the fluid mechanics inside microchannels. Reynolds number is defined as the ration of inertial forces to viscous forces in the fluid, and expressed as follows:

$$\mathrm{Re} = \frac{\mathbf{v}d}{\nu} \tag{4}$$

where d is the characteristic length of the geometry (diameter in this case.), v (m/s) is the fluid velocity, and v (m²/s) is the dynamic viscosity.

The efficiency of mixing η_{mix} of any component (x) at the pipe exit can be calculated using the surface integrals according to the following formula:

$$\eta_{\mathrm{mix}} = 1 - \frac{\iint_R [x] - [x]_\infty \, dA_c}{\iint_R [x]_i - [x]_\infty \, dA_c} \tag{5}$$

where [x] is the concentration of component x as a function of the depth and the width of the channel; $[x]_\infty$ is the concentration of component x after complete mixing; $[x]_i$ is the concentration of component x at the inlet (prior to mixing), and A_c is the cross-sectional area of the exit channel.

3. Fabrication of the microfluidic system

A T-shaped microfluidic mixing design was fabricated to study the decolorization of dyes. The design was drawn in AutoCAD® (Autodesk 2015) as shown in Fig. 1a and fabricated in a poly methyl methacrylate (PMMA) sheet using a laser cutting machine (META 1.5C, TLM Laser Ltd, Worcestershire, UK). The dimensions of the microfluidic channels were (400 ± 0.5) μm width and (680 ± 0.5) μm depth. The serpentine length was 421 mm with a spacing of 1.6 mm. This provided an overall surface area of 180 mm². The volume of the microchip was found to be about 125 mm³. The laser beam velocity and percentage power were manipulated to obtain the desired 680 μm depth for the microfluidic system channels. The parameters were set to be 10 mm/s working velocity and 30% percentage power. Inlets and outlet were drilled using CNC milling machine (DATRON Technology Limited, Milton Keyne, UK) then 1 mm ID brass rods fittings were glued at both of the inlets and the outlet using epoxy glue to avoid leakage. Finally, the chip was sealed using a PVC clear lamination (TMI. LLC, Pittsburgh, USA).Fig. 1b shows the fabricated microfluidic chip for the Fenton process.

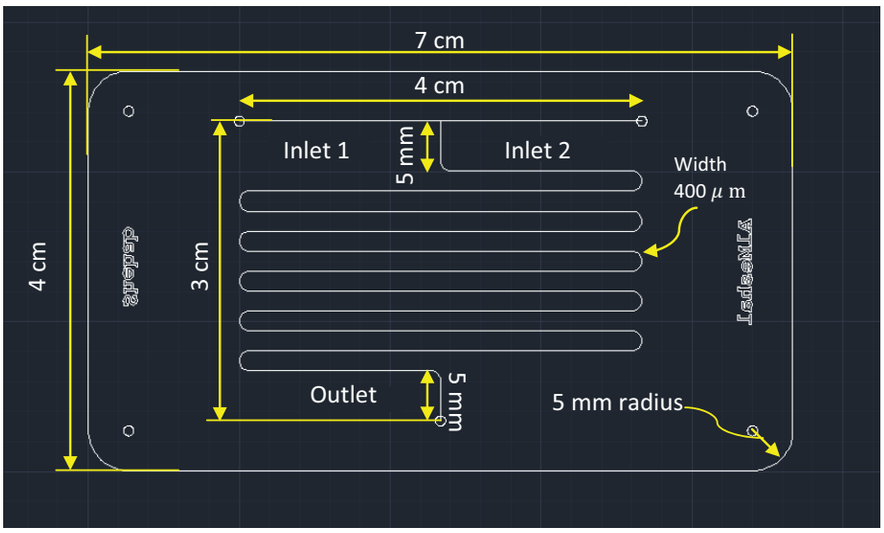

Fig. 1. 2D- AutoCAD drawing for the fabricated microfluidic system.

4. Materials and experimental setup

4.1. Materials

The chemicals used in this study were: Reactive Yellow 181 (P2RN/181, Ciba Specialty Chemicals, Basel, Switzerland), Reactive Blue 19 (RB19, Town End Plc., Leeds, UK), Hydrogen peroxide solution (35 wt. %, Scharlau, Germany), Hydrochloric acid (37 wt. %, Scharlau, Germany), and Ferrous sulfate $FeSO_4$ (Timstar Laboratory Suppliers ltd, UK).RB and RY were used as models for reactive dyes. RY has the following chemical formula: $C_{24}H_{24}ClN_9O_{12}S_3{\cdot}3Na$, with λ_{max} = 414 nm, while RB chemical formula is $C_{22}H_{16}N_2Na_2O_{11}S_3$ with λ_{max} = 592 nm.

4.2. Experimental setup

The fabricated microfluidic chip has two inlets: one inlet (inlet 1) was used for pumping ferrous sulfate and dye aqueous solution) and the other inlet (inlet 2) was used to deliver hydrogen peroxide aqueous solution. All experiments were run at a controlled room temperature of and equal inlet flow rates of 20 µL/s using peristaltic pump (Cole-Parmer Variable Flow pump, UK, Model: EW-73160-40), as demonstrated in Fig. 2 unless otherwise stated.

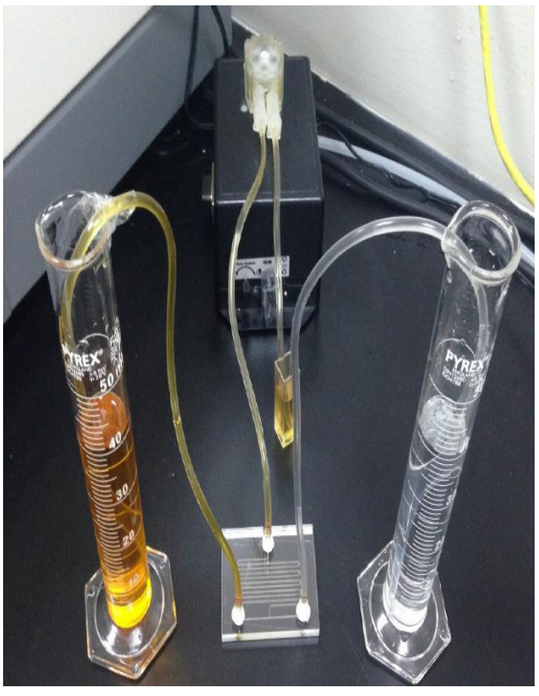

Fig. 2. Experimental setup to deliver a flow rate of 20 µL/s in each inlet of ferrous sulfate and dye aqueous solution (LHS inlet) and hydrogen peroxide aqueous solution (RHS inlet) of the microfluidic chip.

5. Methodology: experimental design

5.1. Procedure

The reactant species were fed to the microreactor as described in section 4.2. The concentrations at different conditions were measured using the UV-Vis spectrophotometer at maximum absorption wavelength for each dye. The absorption was then correlated to the concentration using the Beers Lambert Law and the decolorization efficiency was calculated using the following equation:

$$\%\ \text{Decolorization} = \frac{\text{Initial dye absorbance-Final dye absorbance}}{\text{Initial dye absorbance}} \times 100 \quad (6)$$

5.2. Optimization of process variables

Using the DoE approach, the Central Composite Design (CCD) method was implemented with 28 batch experiments, including four repetitions at the central points, for both tested dyes: reactive yellow and reactive blue, in order to find the optimum conditions of the experiment. These variables (termed as factors; F, in CCD modelling) are: ini-

tial concentration of the dye $[Dye]_o$, ppm, initial concentration of hydrogen peroxide solution $[H_2O_2]_o$, mM, initial concentration of Ferrous sulfate solution $[Fe^{2+}]_o$, mM, and pH. Table 1 (for reactive yellow dye) and Table 2 (for reactive blue dye) illustrate the coding levels for each variable based on the ranges of the operational conditions.

5.3. Experimental design for the kinetic study

In order to simulate the microfluidic system using CFD software, a kinetic model must be provided. However, the Fenton process has many reaction steps [17–21], which complicates the reaction rate expressions. Hence, an empirical model has been implemented in this work to validate the results within the operational range.

The study was conducted using 15 experiments for each dye with 1) changing the initial concentration of the dye, the Fenton reagent, and hydrogen peroxide, as shown in Table 3, and 2) calculating the initial rates of reactions at the operating conditions.

For continuous decolorization experiments, Full Factorial design, 2^3 (=8) experiments were conducted for each dye. The factors were: inlet concentration of the dyes, inlet concentration of hydrogen peroxide, and inlet concentration of ferrous sulfate. A system of codes was used to indicate the level of each factor. These code levels are positive and negative to represent the low and high value, respectively, as shown in Table 4. These values represent the inlet concentrations of ferrous sulfate and dye aqueous solution (inlet 1) and hydrogen peroxide aqueous solution (inlet 2) with equal inlet volumetric flow rates. The pH was chosen to be 3 in all runs following based on the batch experiment results and literature [18,22].

5.4. CFD simulations of the process

For the designed microchip, CFD computation was primarily used to firstly validate the experimental model and reaction kinetics (refer to section 6.6) and secondly, to study the mixing efficiency in the microfluidic system. For the microchip, CFD computation was primarily used to firstly validate the experimental model and reaction kinetics (section 6.6) and secondly, to study the mixing efficiency in the designed microfluidic system (section 6.5). CFD models were run using COMSOL® Multiphysics (version 5) which applies the Finite Element Method (FEM) to solve complicated problems combining several chemical and physical phenomena and processes. All models were run using Windows 7 with Intel® Core™ i5 CPU, 6 GB RAM, and 64-bit Operating System. The models were meshed with normal element size that consumes about 45 min per model.

Table 1
Factors, their level codes, and their real experimental value for batch operation for RY

Variable	Name	Coded levels				
		–2	–1	0	1	2
		Real experimental values				
F_1	$[Dye]_o$/ppm	5	10	15	20	25
F_2	$[H_2O_2]_o$/mM	5	15	25	35	45
F_3	$[Fe^{2+}]_o$/mM	0.02	0.22	0.42	0.62	0.82
F_4	pH	2	2.5	3	3.5	4

Table 2
Factors, their level codes, and their real experimental value for batch operation for RB

Variable	Name	Coded levels				
		–2	–1	0	1	2
		Real experimental values				
F_1	$[Dye]_o$/ppm	10	15	20	25	30
F_2	$[H_2O_2]_o$/mM	7.5	15	22.5	30	37.5
F_3	$[Fe^{2+}]_o$/mM	0.25	0.5	0.75	1	1.25
F_4	pH	1.4	1.8	2.2	2.6	3

6. Results and discussion

6.1. Calibration data of dyes

Two calibration curves were done for reactive yellow (Absorbance = 0.0180 [RY] + 0.0014) and for reactive blue (Absorbance = 0.0125 [RB] + 0.0168). A straight line fit was obtained in both cases with correlation factors R^2 of almost 1 in both sets, indicating excellent agreement with the Beer-Lambert Law.

Table 4
Factors, their level codes, and their real experimental value

Variable	Name	Coded levels	
		–	+
F_1	$[Fe^{2+}]_o$/mM	0.4	1.6
F_2	$[H_2O_2]_o$/mM	10	70
F_3	$[Dye]_o$/ppm	100	200

Table 3
Experimental design for kinetic study

$[Dye]_0$,ppm	25	50	75	100	125	100					100				
$[Fe^{2+}]_o$, mM	0.8					0.2	0.4	0.6	0.8	1	0.8				
$[H_2O_2]_0$, mM	35					35					5	15	25	35	45

6.2. Optimization results

Counter plots with spectrum color level were used to illustrate the effect of several combinations of factors on the decolorization of the individual dye after 20 min running time. The results from these plots lead to the estimation of the kinetic model for the study presented in section 6.3. Fig. 3 shows the effect of Fe(II) concentration and pH on decolorization efficiency, at which the violet color area represents the highest decolorization efficiency at [Fe^{2+}] of 0.8 mM and pH of 3.0. Another optimum region (smaller violet spot) was found at the same pH but with [Fe^{2+}] = 0.4 mM, suggesting efficient decolorization of RY even at low Fe(II) concentration.

The value of pH is critical in Fenton's process. Many researchers suggested optimum initial pH range of 3 to 3.5 for Fenton's process, which agrees with the current results. pH values other than 3 reduces the decolorization efficiency as summarized in Table 5.

Similarly, Fig. 4 illustrates the effect of H_2O_2 and pH combination on the decolorization efficiency, where one violet spot occurs only at pH = 3.0 and [H_2O_2] = 45 mM. However, Fig. 5 shows another optimum concentration for H_2O_2 at 25 mM and [Fe^{2+}] of 0.8 mM.

For reactive blue, the decolorization was investigated after 5 min. Fig. 6 shows best decolorization at a pH range of 2.5–3.0 and Fe(II) concentration range of 0.6–1.1 mM. Almost the same optimization pattern was found in Fig. 7 with the same pH range and H_2O_2 concentration range of 15–30 mM. On the other hand, Fig. 8 suggests optimum conditions to be around 0.9 to 1.1 mM Fe(II) and 25 to 35 mM and 12–17 mM H_2O_2 concentration.

Identifying the optimum ranges as illustrated above helps in developing the kinetics model for the processes, as presented in the coming section.

Based on the optimum ranges of the experimental variables, the percentages of decolorization in the microfluidic system were illustrated for different runs, using cube plot as shown in Fig. 9. Fig. 9a shows the RY decolorization results, where the highest percentage of decolorization was found to be 92.8% at 1.6 mM Fe(II), 70 mM H_2O_2, and 100 ppm RY while the lowest value was 38.7%, found at 0.4 mM Fe(II), 10 mM H_2O_2, and 200 ppm. Fig. 9b shows the results of RB decolorization. The highest decolorization efficiency was found to be 96.0% at 1.6 mM Fe(II), 70 mM H_2O_2, and 100 ppm RB while the lowest efficiency was 21.0% at 0.4 mM Fe(II), 10 mM H_2O_2, and 200 ppm RB.

6.3. Kinetic model results

The initial rate of reaction related to the initial concentration of dye, Fe(II), and H_2O_2 was fitted using the Lagrange numerical differentiation method:

$$-r_{Dye} = \frac{d[Dye]}{dt} \approx [Dye]_1 \frac{2t - t_2 - t_3}{(t_1 - t_2)(t_1 - t_2)} + [Dye]_2 \frac{2t - t_1 - t_3}{(t_2 - t_1)(t_2 - t_3)} + [Dye]_3 \frac{2t - t_1 - t_2}{(t_3 - t_1)(t_3 - t_2)} \quad (7)$$

A rational empirical model was selected to fit the data since it is more realistic and closer to the mechanistic model. The data were fitted to the model using Matlab® cf tool.

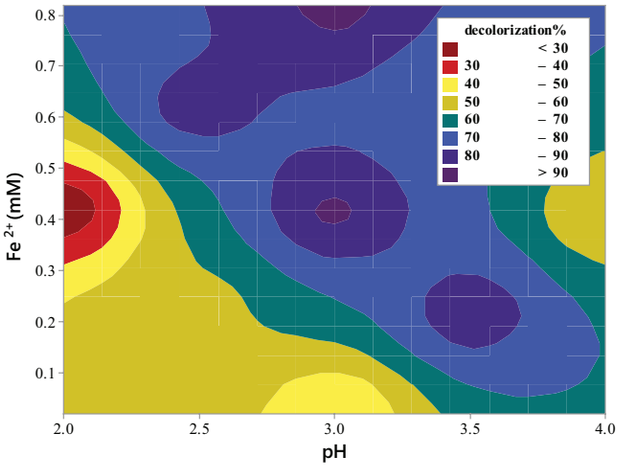

Fig. 3. Counter plot that shows the optimum Fe(II) concentration and pH combination for maximum RY decolorization efficiency.

Table 5
Possible reasons for the reduction in decolorization efficiency in Fenton's process at other than pH = 3

Reason	Reference
When pH < 3	
• Fe^{2+} form stable complexes with H_2O_2	[23]
• Formation of oxonium ion $H_2O_2 + H^+ \rightarrow H_3O_2^+$	
• Formation of oxonium ions which enhance the stability of H_2O_2	
• Increasing the rate of Eq. (R6), therefore increasing Fe^{3+} concentration which terminates the Fe(II)/Fe(III) cycle.	[18]
When pH < 3~3.5	
• Formation of ferric oxyhydroixde precipitate which reduces the concentration of Fe(II) ions in the solution	[18]
• At pH above 6, the following reaction occurs: $Fe^{3+} + 3OH^- \rightarrow Fe(OH)_3$, and ferric hydroxide decomposes H_2O_2 into H_2O and O_2.	[22]
• At pH above 5, ferrous ions favor to exist as which reacts slower with H_2O_2.	
• Auto-decomposition of $H_2O_2 \rightarrow H_2O + 1/2\ O_2$	[24]
• The concentration of hydroperoxy increases which sinks the OH radicals, as follows: $H_2O_2 \rightleftharpoons H^+ + HO_2^-$ $^{\bullet}OH + HO_2^- \rightarrow H_2O + {}^{\bullet}O_2^-$	

6.3.1. Reactive yellow

The results of fixing the initial concentration of Fe(II) and H_2O_2, while changing the initial concentration of RY are illustrated in Fig. 10. The data were fitted using (1/1) rational model, with R^2 of 0.95 of the data captured by the model.

Fig. 11 illustrates the results obtained from varying H_2O_2 concentration between 5 to 45 mM at constant RY concentration and Fe(II). The optimum H_2O_2 concentration

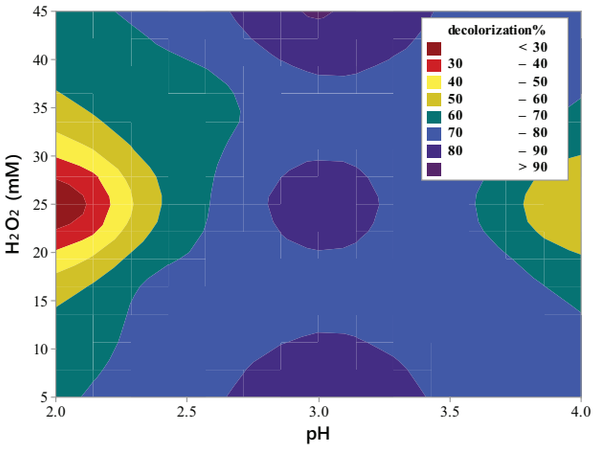

Fig. 4. Counter plot shows the optimum [H_2O_2] and pH combination for maximum RY decolorization efficiency.

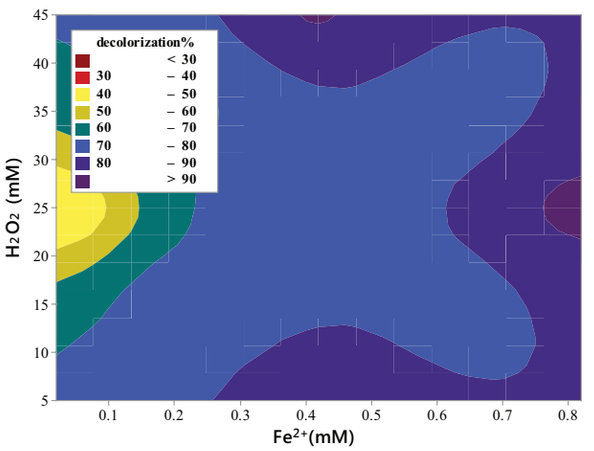

Fig. 5. Counter plot shows the optimum hydrogen peroxide and Fe(II) concentration combination for maximum RY decolorization efficiency.

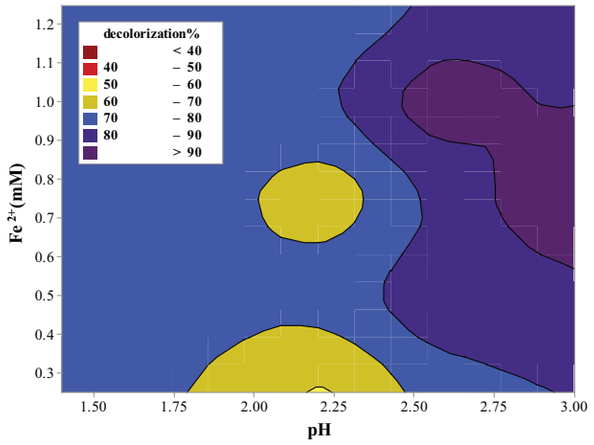

Fig. 6. Counter plot shows the optimum Fe(II) concentration and pH combination for maximum RB decolorization efficiency.

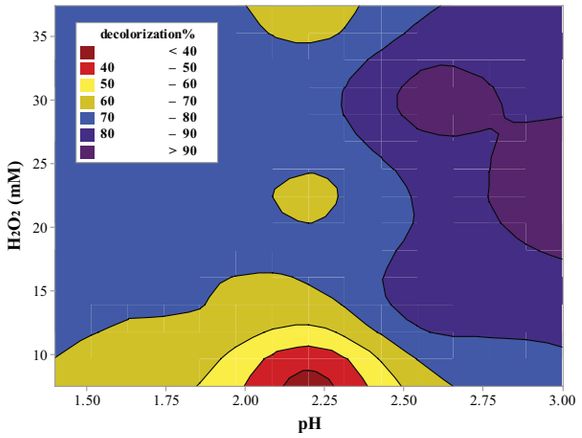

Fig. 7. Counter plot shows the optimum hydrogen peroxide concentration and pH combination for maximum RB decolorization efficiency.

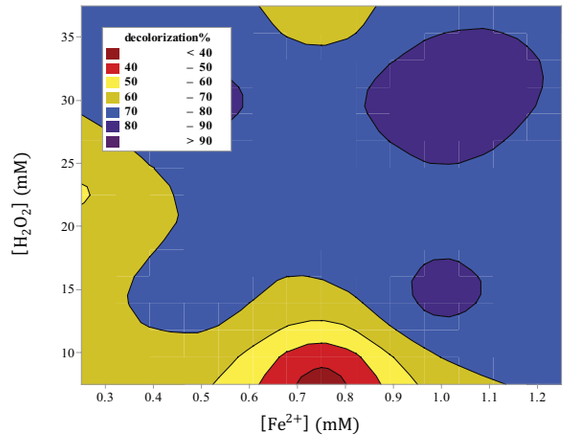

Fig. 8. Counter plot shows the optimum hydrogen peroxide and Fe(II) concentration combination for maximum RB decolorization efficiency.

was found to be 35 mM. The data were fitted using (1/2) rational model, with $R^2 = 0.998$ of the data captured by the model.

Finally, fixing RY and H_2O_2 concentrations while changing the Fe(II) concentration from 0.2 to 1 mM gave the results illustrated in Fig. 12. It was found that increasing the Fe(II) concentration increases the decolorization rate. However, an optimum concentration of Fe(II) was found to be at 1 mM Fe(II). The rate was fitted using (1/2) rational model with $R^2 = 0.997$ of the data captured by the model.

The operating conditions and the kinetic model results are summarized in Table 6, along with the overall rate of reaction.

6.3.2. Reactive blue

The same procedures were followed with RB. Fig. 13 to Fig. 15 present the rate of reaction profiles. The results of fix-

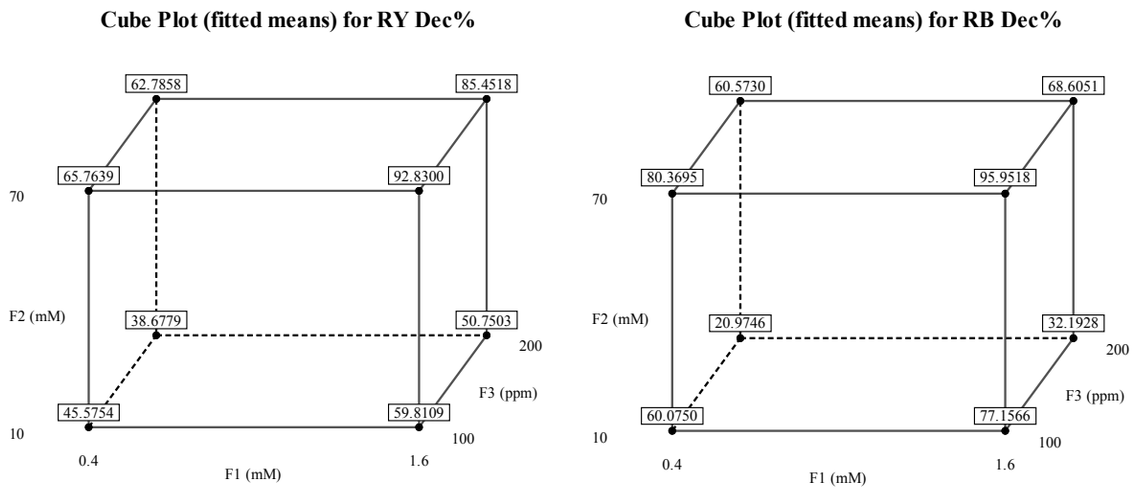

Fig. 9. Decolorization efficiencies in the microfluidic system using homogenous Fenton reagent at different conditions for a) RY and b) RB. F1, F2, F3 definitions and ranges are as given in Table 1 for RY and Table 2 for RB.

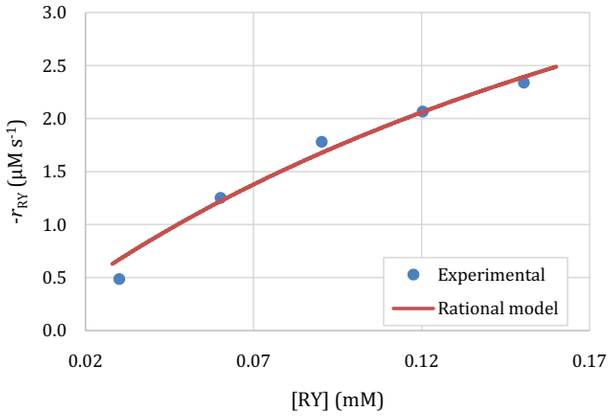

Fig. 10. Fitting the initial rate of RY decolorization to the initial RY concentration using rational empirical model (R^2 = 0.950).

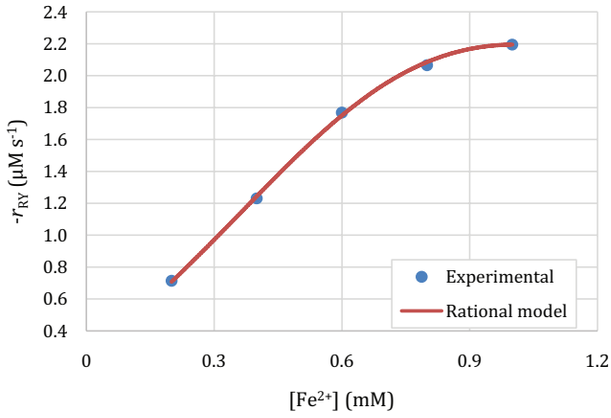

Fig. 12. Fitting the initial rate of RY decolorization to the initial Fe(II) concentration using rational empirical model (R^2 = 0.997).

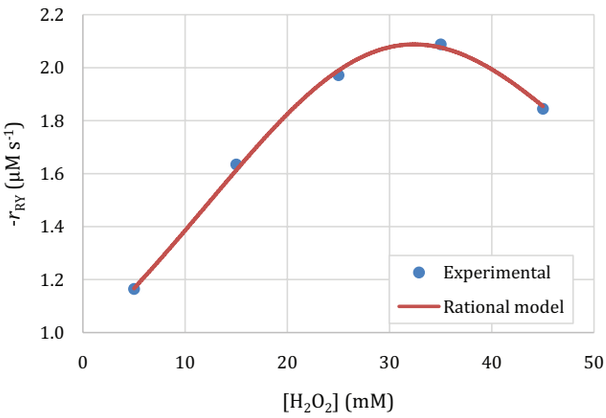

Fig. 11. Fitting the initial rate of RY decolorization to the initial H_2O_2 concentration using rational empirical model (R^2 = 0.998).

ing the initial concentration of Fe(II) and H_2O_2, while changing the initial concentration of RB are illustrated in Fig. 13. The data were fitted using (1/1) rational model, with R^2 of 0.931 indicating 93.1% of the data captured by the model. The optimum H_2O_2 concentration was found to be 35 mM, with data fitted using (1/2) rational model and R^2 = 0.946, while the optimum concentration of Fe(II) was found to be 0.8 mM Fe(II), with data fitted using (1/2) rational model and R^2 = 0.999. The kinetic model results at the optimum operating conditions are summarized in Table 7 along with the overall rate of reaction.

6.4. Effect of variables on the decolorization process

This section discusses the effect of $[Dye]_o$, $[Fe(II)]_o$, and $[H_2O_2]_o$ on the decolorization efficiency for the Fenton process that was conducted in the fabricated microfluidic system.

Table 6
Kinetic model results for the decolorization of reactive yellow

Dye	Fixed variables	Varied variable	Range	Reaction rate	Model	R^2
Reactive Yellow	$[Fe(II)]_o$ $[H_2O_2]_o$	$[RY]_o$	0.03–0.15 mM	$-r_{RY1} = 6.663\times10^{-3}\frac{[RY]}{[RY]+0.2684}$	(1/1) rational model	0.950
	$[Fe(II)]_o$ $[RY]_o$	$[H_2O_2]_o$	5–45 mM	$-r_{RY2} = 1.608\times10^{-2}\frac{[H_2O_2]+118.6}{[H_2O_2]^2-57.12[H_2O_2]+1963}$	(1/2) rational model	0.998
	$[H_2O_2]_o$ $[RY]_o$	$[Fe(II)]_o$	0.2–1 mM	$-r_{RY3} = 1.901\times10^{-3}\frac{[Fe^{2+}]+0.1600}{[Fe^{2+}]^2-1.152[Fe^{2+}]+1.156}$	(1/2) rational model	0.997

Overall rate of reaction: $-r_{RY} = \frac{a_1[RY]([H_2O_2]+a_2)([Fe^{2+}]+a_3)}{([RY]+a_4)([H_2O_2]^2+a_5[H_2O_2]+a_6)([Fe^{2+}]^2+a_7[Fe^{2+}]+a_8)}$

a_1	a_2	a_3	a_4	a_5	a_6	a_7	a_8
4.707×10^{-2}	118.6	0.1600	0.2684	–57.12	1963	–1.152	1.156

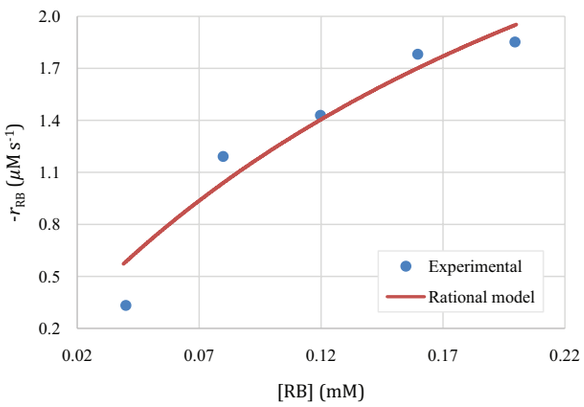

Fig. 13. Fitting the initial rate of RB decolorization to the initial RB concentration using rational empirical model (R^2 = 0.931).

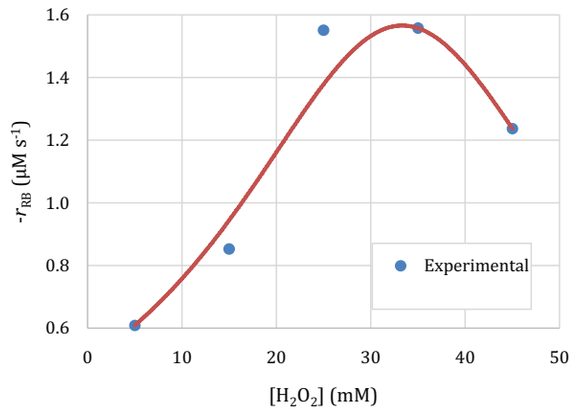

Fig. 14. Fitting the initial rate of RB decolorization to the initial H_2O_2 concentration using rational empirical model (R^2 = 0.946).

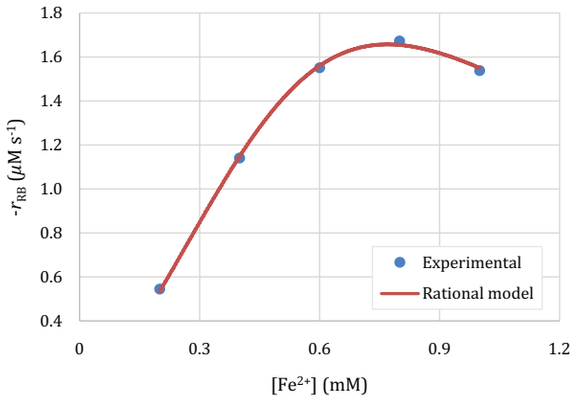

Fig. 15. Fitting the initial rate of RB decolorization to the initial Fe(II) concentration using rational empirical model (R^2 = 0.999).

6.4.1. Effect of H_2O_2 concentration

As hydrogen peroxide concentration increases more OH radicals are available in the process. This subsequently increases the rate of decolorization up to a certain limit (35 ppm in both dyes), as shown in Fig. 12 (for RY) and Fig. 15 (for RB). Further increase in the H_2O_2 concentration leads to lowering the decolorization efficiency. This is mainly due to the increase in •OH scavenging rate at higher concentrations where H_2O_2 acts as a quencher according to the following possible reactions: [18,23–26].

$$H_2O_2 + {}^{\bullet}OH \rightarrow H_2O + {}^{\bullet}O_2H \quad (8)$$

$${}^{\bullet}OH + {}^{\bullet}OH \rightarrow H_2O_2 \quad (9)$$

$${}^{\bullet}OH + {}^{\bullet}O_2H \rightarrow H_2O + O_2 \quad (10)$$

Table 7
Kinetic model results for the decolorization of reactive blue

Dye	Fixed variables	Varied variable	Range	Reaction rate	Model	R^2
Reactive Blue	$[Fe(II)]_o[H_2O_2]_o$	$[RB]_o$	0.04–0.2 mM	$-r_{RB1} = 4.689\times10^{-3}\frac{[RB]}{[RB]+0.2804}$	(1/1) rational model	0.931
	$[Fe(II)]_o[RB]_o$	$[H_2O_2]_o$	5–45 mM	$-r_{RB2} = \frac{0.8004}{[H_2O_2]^2-66.68[H_2O_2]+1623}$	(1/2) rational model	0.946
	$[H_2O_2]_o[RB]_o$	$[Fe(II)]_o$	0.2–1 mM	$-r_{RB3} = 1.277\times10^{-3}\frac{[Fe^{2+}]}{[Fe^{2+}]^2-0.7687[Fe^{2+}]+0.5924}$	(1/2) rational model	0.999

Overall rate of reaction: $-r_{RB} = \frac{b_1[RB][Fe^{2+}]}{([RB]+b_2)([H_2O_2]^2+b_3[H_2O_2]+b_4)([Fe^{2+}]^2+b_5[Fe^{2+}]+b_6)}$

b_1	b_2	b_3	b_4	b_5	b_6
1.796	0.2804	–66.68	1623	–0.7687	0.5924

6.4.2. Effect of Fe^{2+} concentration

Referring to the following initiation reaction [19],

$$Fe^{2+} + H_2O_2 \rightarrow Fe^{3+} + {}^{\bullet}OH + OH^- \quad (11)$$

It is obvious that increasing Fe(II) concentration increases the rate of formation of the •OH radicals, which leads to better decolorization efficiency up to specific limits (1 mM and 0.8 mM, for RY and RB, respectively), as shown in Fig. 10 (for RY) and Fig. 13 (For RB). Any further increment in Fe^{2+} concentration decreases the rate of decolorization due to scavenging of •OH radicals according to the following equation: [3,17,19,22,26].

$$Fe^{2+} + {}^{\bullet}OH \rightarrow Fe^{3+} + OH^- \quad (12)$$

The Fe(II)/H_2O_2 molar ratio experimental results illustrated in section 6.2 shows a good agreement with the literature [27], which was about 0.02 and 0.025 with RB and RY, respectively, compared to the current optimum ratio of 0.023 and 0.028 with RB and RY, respectively obtained in this study.

6.4.3. Effect of initial dye concentration

Generally, the decolorization efficiency is inversely proportional to the initial dye concentration. m, the rate of reaction is directly proportional to the initial dye concentration [14].

6.5. CFD mixing efficiency study

A comprehensive study was made on the mixing efficiency in the microfluidic system. Efficient mixing is a crucial requirement to validate the model. Mixing in the microfluidic channel is mainly governed by diffusion, where laminar flow helps improving the mixing efficiency. Furthermore, having sinusoidal serpentines provides chaotic advection to enhance the rate of diffusion, as discussed by many authors [28,29]. In this study, mixing was induced passively using the serpentine to ensure good level of mixing. The results shows that a 400 µm ID channel needs a total length of at least 400 mm to achieve 99% mixing efficiency, at the operated flow rate.

Two models were run using COMSOL, in order to evaluate the mixing efficiency in the microfluidic system. The inlet conditions were chosen to be 100 ppm, 1.6 mM, and 70 mM for $[Dye]_o$, $[Fe^{2+}]_o$, and $[H_2O_2]_o$, respectively, diffusion coefficients: $D_{Fe2+} = 7.19\times10^{-10}m^2/s$ [30], $D_{H2O2} = 1.71\times10^{-5}$ cm^2/S [31], and dyes diffusion coefficient using the empirical Wilke-Chang equation (Eq. (4)) at a room temperature of 25. The CFD solves the laminar flow (fluid mechanics) module, with an inlet flow rate of 20 µL/s and transport fluid module with diluted species (mass transfer) simultaneously. The mixing efficiency of the reacted species is summarized in Table 8.

The results clearly agree with Fick's law of diffusion, where the diffusion coefficient increases with the increase in the diffusion rate leading, to an increase in the mixing efficiency. It was also expected to have the highest mixing efficiency with H_2O_2 due to its highest diffusion coefficient and concentration while having lowest diffusion coefficient with RY which leads to lowest mixing efficiency [32,33]. A sample model for COMSOL results is shown in Fig. 16, where $[RY]_o$ = 200 ppm (0.24 mM), and inlet flow rate of 20 µL/s.

Introducing serpentines in the designed microfluidic system was mainly to 1) reduce the design area and to, most importantly, 2) improve the mixing efficiency. This could be evident in Fig. 17 where a higher range of concentration gradient takes place in the serpentine region over elsewhere in the channels.

Table 8
Summary of mixing efficiency results using CFD models for the involved species

	RY	RB	Fe(II)	H_2O_2
Diffusion Coefficient (m^2/s)	2.98×10^{-10}	3.59×10^{-10}	17.1×10^{-10}	7.19×10^{-10}
Inlet concentration (mM)	0.24	0.32	1.6	35
η_{mix} (%)	98.7	99.5	99.8	100.0

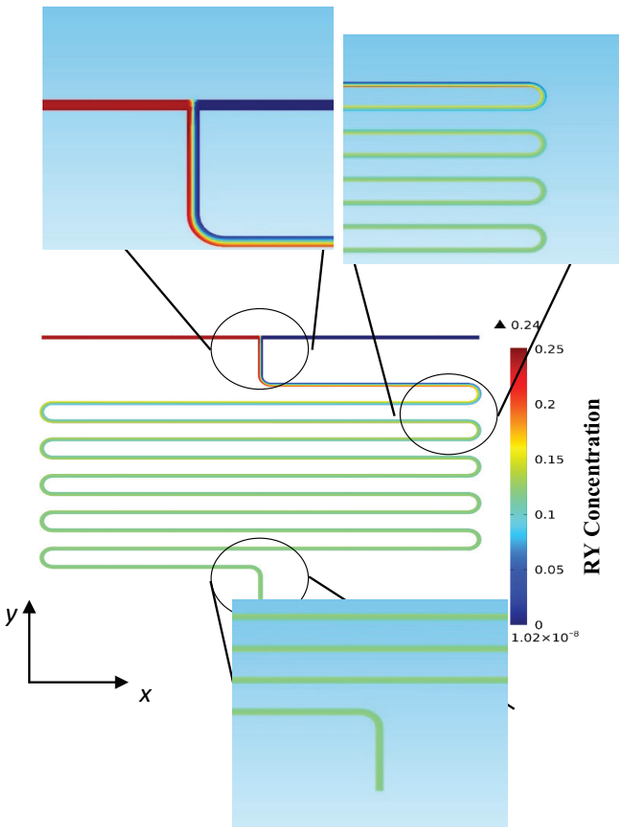

Fig. 16. A sample model for the concentration gradient of Reactive yellow in the designed microfluidic system.

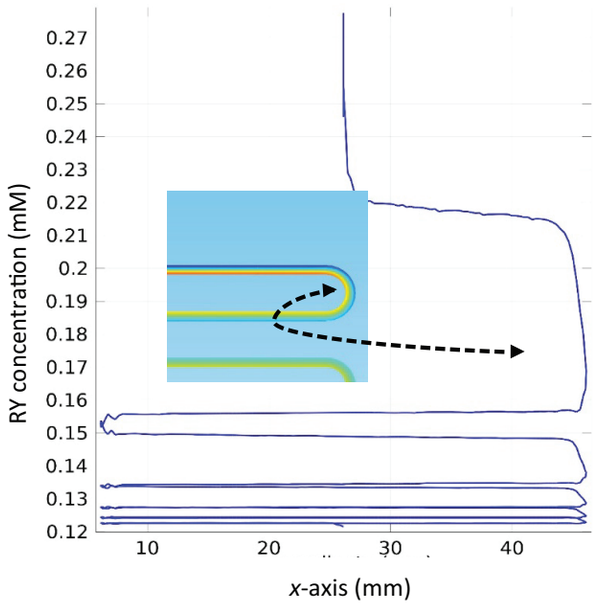

Fig. 17. The effect of serpentines in the microfluidic system on the mixing efficiency.

6.6. CFD results for the decolorization of the studied reactive dyes

The decolorization reactions were also simulated by CFD to test their agreement with the experimental results. The overall CFD results for all runs (refer to Table 9) are summarized in Fig. 18 for RY (Fig. 18a) and RB (Fig. 18b), in comparison to those obtained experimentally. Good agreement between the experiments and CFD results is shown for both dyes at almost all operating conditions. The deviation observed in runs (*b*) and (*ab*) for RY, and runs (*1*) and (*ab*) for RB, is probably due to the high ratio of to which was calculated as 0.16, compared to the optimum ratio found in literature, as detailed previously. At the optimum operating conditions (run *bc*) though, the error was found to be 1.08% and 3.85% only, for RY and RB, respectively. This confirms the validity of the proposed kinetic model for the studied dyes.

Table 9
Coding system for the microfluidic chip experiments

	[Dye]/ppm (A)		[Fe (II)]/ mM (B)		[H_2O_2]/ mM (C)	
	Coded	Uncoded	Coded	Uncoded	Coded	Uncoded
(1)	–	100	–	0.4	–	10
a	+	200	–	0.4	–	10
b	–	100	+	1.6	–	10
c	–	100	–	0.4	+	70
ab	+	200	+	1.6	–	10
bc	–	100	+	1.6	+	70
ac	+	200	–	0.4	+	70
abc	+	200	+	1.6	+	70

A sample CFD result for the decolorization gradient in the microfluidic chip of each dye is shown in Fig. 19. The selected run was (*bc*), according to Table 9, i.e. with inlet concentrations of 100 ppm dye, 1.6 mM Fe(II) , 70 mM H_2O_2, and inlet flow rate of 20 µL/s. COMSOL results show that the concentration of RY (Fig. 19a) decreases from 0.12 mM to 0.0086 mM, while that of RB

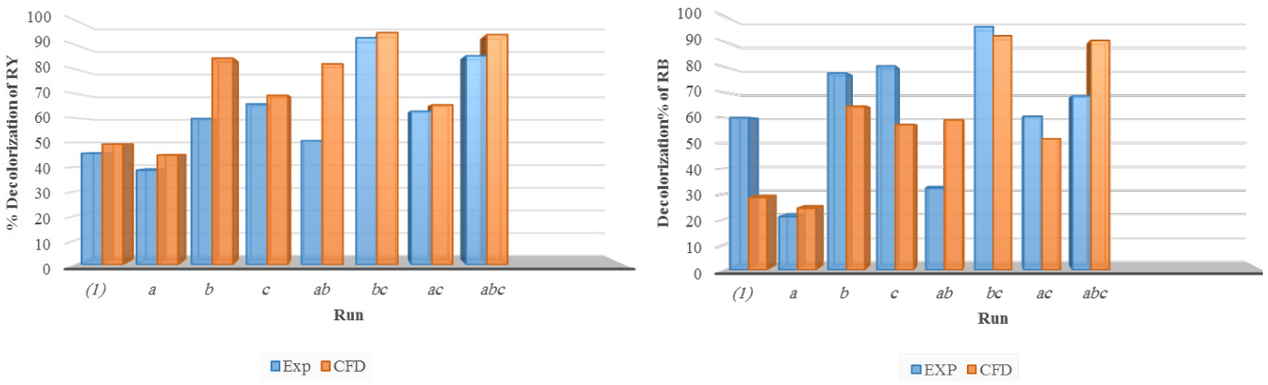

(a) (b)

Fig. 18. The CFD results in comparison with the experimental results of a) RY decolorization, and b) RB decolorization.

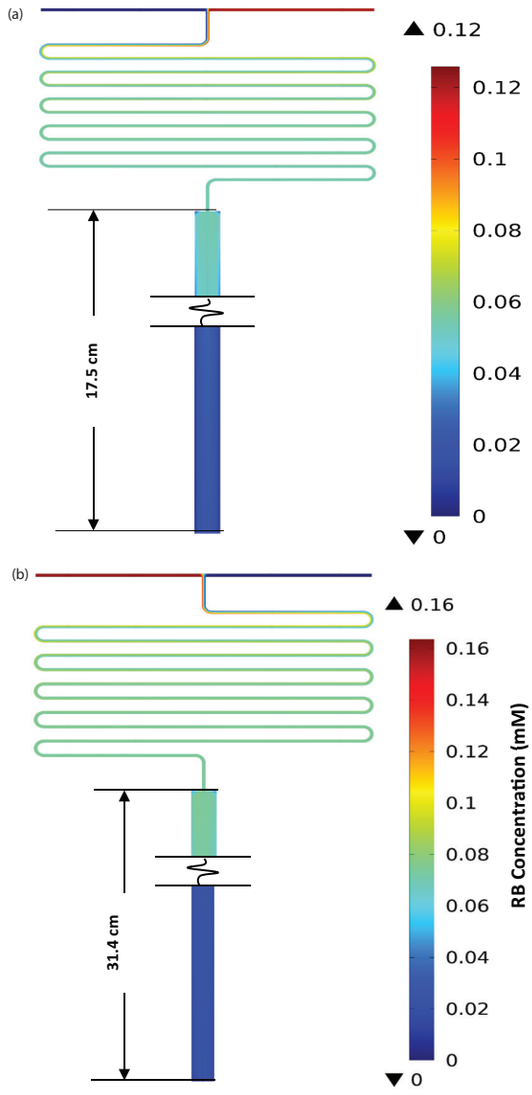

Fig. 19. CFD results for the decolorization of a) RY and b) RB, following (*bc*) run, with an inlet flow rate of 20 µL/s.

decreases from 0.16 mM to 0.0123 mM (Fig. 19b) along the microfluidic T- shaped serpentine, which lead to percentage decolorization of 92.8 and 92.3% for RY and RB, respectively.

7. Conclusions

Successful mathematical and experimental modeling for reactive dyes decolorization using the Fenton oxidation process in a microfluidic system was presented. Reactive yellow and reactive blue dyes were used as models. For both dyes, good agreement was obtained between both experimental and mathematical modeling results. These results were also validated with additional computational fluid dynamic studies.

The Fenton oxidation process was optimized in batch mode and the optimum conditions were found to be 0.8 mM, 35 mM, and 3.0 for Fe(II) concentration, H_2O_2 concentration, and pH, respectively. Initial rate study was conducted with 15 experiments per dye, with rational model that captures 95 and 93% of the data, for RY and RB, respectively. The highest decolorization percentage using the Fenton process in the microfluidic system was found to be 92.9 and 96.0% for RY and RB, respectively, at 100 ppm inlet dye concentration, 1.6 mM inlet Fe(II) concentration, 70 mM H_2O_2 inlet concentration, 3.0 pH (after mixing) , and 20 µL/sinlet flow rate. Kinetic models were also developed for the Fenton oxidation process, on the studied dyes. The rate of reaction expressions proved to give valid results over the experimental ranges of $[RY]_o$ = 0.03–0.15 mM, $[RB]_o$ = 0.04–0.2 mM, $[H_2O_2]_o$ = 5–45 mM, and $[Fe(II)]_o$ = 0.2–1 mM.

Finally, the mixing efficiency studied using CFD modelling revealed that more than 98.7% mixing efficiency was obtained after ten serpentines (total channel length of 420 mm). CFD results for the decolorization efficiency of the studied process was found to be 92.8% for RY after 200 s which deviates by 1.08% only from the experimental value, at the optimum operating conditions. As for RB, the decolorization efficiency was found to be 92.3% after 200 s which deviates by 3.85% only from the experimental value, at the optimum operating conditions.

References

[1] B. Adinew, Textile effluent treatment and decolorization techniques – a review, Chemistry: Bulg. J. Sci. Edu., 21 (2012) 434–456.

[2] E. Kusvuran, O. Gulnaz, S. Irmak, O.M. Atanur, H.I. Yavuz, O. Erbatur, Comparison of several advanced oxidation processes for the decolorization of Reactive Red 120 azo dye in aqueous solution, J. Hazard. Mater., 109 (2004) 85–93.

[3] S. Meric, D. Kaptan, T. Olmez, Color and COD removal from wastewater containing Reactive Black using Fenton's oxidation process, Chemosphere, 54 (2004) 435–441.

[4] S. Meriç, G. Lofrano, V. Belgiorno, Treatment of Reactive dyes and textile finishing wastewater using fenton's oxidation for reuse, Int. J. Environ. Pollut., 23 (2005) 248–258.

[5] A. Verma, A. Kaur Hura, D. Dixit, Sequential photo-Fenton and sono-photo-Fenton degradation studies of Reactive Black 5 (RB5), Desal. Water Treat., 56 (2015) 677–683.

[6] F. Duarte, V. Morais, F.J. Maldonado-Hódar, L.M. Madeira, Treatment of textile effluents by the heterogeneous Fenton process in a continuous packed-bed reactor using Fe/activated carbon as catalyst, Chem. Eng. J., 232 (2013) 34–41.

[7] F. Trachsel, Design of a Microreactor for Reactions Using Supercritical Fluids as the Reaction Solvent, Institute of Process Engineering, ETH Zurich, ETH Zurich, 2008.

[8] T. Dietrich, Microchemical Engineering in Practice, Wiley, Hoboken, New Jersy, 2009, 174–175.

[9] G. Donati, R. Paludetto, Scale up of chemical reactors, Catal. Today, 34 (1997) 483–533.

[10] R. Jevtic, M. AlDahhan, M.P. Dudukovic, Review of Microreactors, 2007.

[11] M. Rahimi, B. Aghel, M. Sadeghi, M. Ahmadi, Using Y-shaped microreactor for continuous decolorization of an Azo dye, Desal. Water Treat., 52 (2014) 5513–5519.

[12] S. Papić, M. Mužic, N. Koprivanac, I. Peternel, M. Deanović, Decolorization of the anthraquinone dye C. I. Reactive blue 2 by Fenton oxidation; Statistical experimental design, Chem. Biochem. Eng. Quart., 24 (2010) 9–16.

[13] U. Akay, E.A. Demirtas, Degradation of burazol blue ED by heterogeneous fenton process: simultaneous optimization by central composite design, Desal. Water Treat., 56 (2015) 3346–3356.

[14] Y. Shen, Q. Xu, J. Shi, M. Li, Y. Zhang, Optimization and mechanism study of C.I. acid blue 25 wastewater degradation by ozone/fenton oxidation process: Response surface methodology, intermediate products and degradation pathway, Desal. Water Treat., 65 (2017) 313–326.

[15] H. Bruus, Theoretical Microfluidics, 3rd ed., Oxford University Press, Oxford, UK, 2008.

[16] K. Miyabe, R. Isogai, Estimation of molecular diffusivity in liquid phase systems on the basis of the absolute rate theory, Anal. Sci., 29 (2013) 467–472.

[17] J. Shi, Z. Ai, L. Zhang, Fe@Fe_2O_3 core-shell nanowires enhanced Fenton oxidation by accelerating the Fe(III)/Fe(II) cycles, Water Res., 59 (2014) 145–153.

[18] F. Torrades, J. García-Montaño, Using central composite experimental design to optimize the degradation of real dye wastewater by Fenton and photo-Fenton reactions, Dyes and Pigments, 100 (2014) 184–189.

[19] Ö. Gökkuş, F. Çoşkun, M. Kocaoğlu, Y.Ş. Yıldız, Determination of optimum conditions for color and COD removal of Reactive Blue 19 by Fenton oxidation process, Desal. Water Treat., 52 (2014) 6156–6165.

[20] J. Saien, A.R. Soleymani, H. Bayat, Modeling Fentonic advanced oxidation process decolorization of Direct Red 16 using artificial neural network technique, Desal. Water Treat., 40 (2012) 174–182.

[21] K. Sehested, O.L. Rasmussen, H. Fricke, Rate constants of OH with HO_2, O_2^-, and $H_2O_2^+$ from hydrogen peroxide formation in pulse irradiated oxygenated water, J. Phys. Chem., 72 (1968) 626–631.

[22] S. Karthikeyan, A. Titus, A. Gnanamani, A.B. Mandal, G. Sekaran, Treatment of textile wastewater by homogeneous and heterogeneous Fenton oxidation processes, Desalination, 281 (2011) 438–445.

[23] P.V. Nidheesh, R. Gandhimathi, Trends in electro-Fenton process for water and wastewater treatment: An overview, Desalination, 299 (2012) 1–15.

[24] A. Mahmood, S. Ali, H. Saleem, T. Hussain, Optimization for degradation of commercial Reactive Yellow Dye 145 through Fenton's reagent, Asian J. Chem., 23 (2011) 3875–3878.

[25] M. Muruganandham, M. Swaminathan, Advanced oxidative decolourisation of Reactive Yellow 14 azo dye by UV/TiO_2, UV/H_2O_2, UV/H_2O_2/Fe^{2+} processes—a comparative study, Sep. Purif. Technol., 48 (2006) 297–303.

[26] M. Siddique, R. Farooq, G. Price, Synergistic effects of combining ultrasound with the Fenton process in the degradation of Reactive Blue 19, Ultrason. Sonochem., 21 (2014) 1206–1212.

[27] S. Papić, D. Vujević, N. Koprivanac, D. Šinko, Decolourization and mineralization of commercial reactive dyes by using homogeneous and heterogeneous Fenton and UV/Fenton processes, J. Hazard. Mater., 164 (2009) 1137–1145.

[28] M. Nimafar, V. Viktorov, M. Martinelli, Experimental comparative mixing performance of passive micromixers with H-shaped sub-channels, Chem. Eng. Sci., 76 (2012) 37–44.

[29] Y. Fang, Y. Ye, R. Shen, P. Zhu, R. Guo, Y. Hu, L. Wu, Mixing enhancement by simple periodic geometric features in microchannels, Chem. Eng. J., 187 (2012) 306–310.

[30] J. Buffle, Z. Zhang, K. Startchev, Metal flux and dynamic speciation at (bio)interfaces. Part I: Critical evaluation and compilation of physicochemical parameters for complexes with simple ligands and fulvic/humic substances (Supplementary Information), Environ. Sci. Technol., 41 (2007) 7609–7620.

[31] R.C. Peña, J.C.M. Gamboa, M. Bertotti, T.R.L.C. Paixão, Studies on the electrocatalytic reduction of hydrogen peroxide on a glassy carbon electrode modified with a ruthenium oxide hexacyanoferrate film, Int. J. Electrochem. Sci., 6 (2011) 394–403.

[32] V. Hessel, H. Löwe, F. Schönfeld, Micromixers—a review on passive and active mixing principles, Chem. Eng. Sci., 60 (2005) 2479–2501.

[33] C.Y. Lee, C.L. Chang, Y.N. Wang, L.M. Fu, Microfluidic mixing: a review, Int. J. Mol. Sci., 12 (2011) 3263–3287.